PERGAMON

Engineering Fracture Mechanics 68 (2001) 1535–1556

Engineering Fracture Mechanics

www.elsevier.com/locate/engfracmech

Dynamic full field measurements of crack tip temperatures

P.R. Guduru [a], A.T. Zehnder [b], A.J. Rosakis [a,*], G. Ravichandran [a]

[a] *Graduate Aeronautical Laboratories, California Institute of Technology, Mail Stop 105-50, Pasadena, CA 91125, USA*
[b] *Department of Theoretical and Applied Mechanics, Cornell University, Ithaca, NY 14853, USA*

Received 17 October 2000; received in revised form 4 March 2001; accepted 12 March 2001

Abstract

This paper presents a detailed investigation of the evolution of temperature field at the tip of a stationary crack subjected to dynamic loading in two different types of steels. A high speed two-dimensional infrared camera was used to image the temperature fields at the crack tips. In a high strength maraging steel, the thermograms reveal the development of plastic zone and the process of crack initiation and propagation. In ductile HY100 steel, the thermograms are used to estimate the evolution of J integral and its critical value at crack initiation. The temperature images are also used to investigate the dominance of HRR field around the crack tip.

Keywords: Infrared temperature measurement; Dynamic fracture; Crack tip temperature; J integral

1. Introduction

In addition to inertia and strain rate sensitivity effects, the temperature rise at the tip of a stationary crack subjected to dynamic loading could significantly alter its resistance to initiation. As discussed by Freund [1], strain rate and temperature can have opposing effects on the fracture toughness vs. loading rate relation, with higher strain rates resulting in decreasing toughness because of material rate sensitivity and higher temperatures having the opposite effect. If the loading rate were high enough, local heating in a crack tip plastic zone would be nearly adiabatic. The increase in the temperature within the fracture process zone directly affects the micromechanisms of fracture, by modifying the local constitutive relation, resistance to void growth process, etc. Kraft and Irwin [2] attempted to estimate the temperature rise at the crack tip in three different materials, a titanium alloy, a steel and an aluminum alloy, by examining their fracture toughness behavior over a range of loading rates and at different temperatures. The temperature rise they predicted was typically less than 120°C. By treating a growing plastic zone as a distributed source of heat, Rice and Levy [3] estimated that the maximum temperature rise at the tip of a crack at initiation would be 120°C, 60°C and 80°C, respectively, for the above three materials, which was in good agreement with the experimental results. By assuming that the fracture behavior of a specimen at a given temperature would be the same as that of a specimen whose crack tip process zone is at that temperature, they proposed a model

* Corresponding author. Tel.: +1-626-395-4523; fax: +1-626-449-6359.
E-mail address: rosakis@atlantis.caltech.edu (A.J. Rosakis).

0013-7944/01/$ - see front matter
PII: S0013-7944(01)00045-5

to predict the fracture toughness vs. loading rate relation. Their work, for the first time, underlined the importance of considering the effects of temperature rise at the tip of a stationary crack subjected to rapid loading on its fracture resistance. Crack tip temperature as a parameter affecting the fracture processes was also considered by Jha and Narasimhan [4] and by Basu and Narasimhan [5]. Using a 2D plane strain finite element model, employing finite deformations, to analyze crack initiation in 4340 steel, Jha and Narasimhan [4] estimated that the temperature near the crack tip at initiation could be as high as 230°C. In addition, as discussed by Freund [1], temperature at a crack tip could bring about a complete change in the mechanisms of fracture, an effect which was conclusively demonstrated by the experiments of Wilson et al. [6].

In spite of such early analytical and numerical demonstrations of the potentially significant role of the crack tip temperature in determining the mechanisms of fracture, there has been very little effort to accurately measure the evolution of temperature fields at the crack tip. This can be traced to the particular experimental difficulties that would be encountered in such an effort. Typical dynamic crack initiation experiments are very rapid events, happening at time scales ranging from a few tens of microseconds to a few milliseconds at the most. In addition, the size of a typical fracture process zone ahead of a crack tip is of the order of the critical crack opening displacement, which ranges from tens of microns to a few hundreds of microns for most structural materials. Making accurate measurements of such highly dynamic and transient temperatures at such small length scales, severely limits the choice of experimental techniques to either fast response thermocouples or to infrared (IR) thermography. However, even tiny embedded thermocouples of 100 μm bead diameter have a response time of a few hundred microseconds [7], rendering them unsuitable for the current application. Moreover, embedded thermocouples can be highly intrusive and provide only single-point information. Wells [8] was among the first to use thermocouples for temperature measurement in fracture problems. This technique was later refined and used, among others, by Shockey et al. [9] and Rittel [10].

High speed IR detectors have been successfully used in the past by several investigators to measure temperature rise during dynamic deformation in materials. The IR detectors that have been used are of either a single element type or a linear array of 8–16 detectors variety, with each detector averaging temperature over a spot, the size of which ranged from 20 μm to a few hundred microns. However, their use has been limited to experimental situations where the location of the temperature measurement spot did not have to be very precise. In dynamic experiments, it is nearly impractical to focus these detectors at a tiny spot such as a crack tip process zone, due to high speed impact induced vibrations and deformation and thus are not very suitable for crack tip temperature measurement. One way to effectively overcome such problems would be to use a 2D IR camera with a high speed data acquisition capability and with a spatial resolution of the order of 100 μm. We explore this idea in the current investigation.

In addition to the significance of crack tip temperatures mentioned above, temperature fields within the crack tip plastic zone could potentially be used as a diagnostic tool to measure the crack tip loading parameters such as the dynamic J integral, under certain conditions. By identifying the critical time of crack initiation, the critical value of J integral can then be inferred. This idea was introduced and explored by Guduru et al. [11] by deriving a relation between the J integral and the crack tip temperature field using the HRR singular field [12,13] within the plastic zone and assuming adiabatic conditions. They used a single element HgCdTe IR detector, to measure the average temperature rise over an area of 300×300 μm^2 on the specimen in front of the crack tip, and used it to estimate the evolution of the J integral in a drop weight impact experiment on HY100 steel in a three-point bend configuration. Despite the novelty of the experimental technique, the accuracy of their measurement was limited by the relatively large area of temperature averaging, uncertainty in locating the area of measurement in relation to the crack tip and the rigid translation of the specimen during deformation. In order to pursue this idea further by transcending the stated limitations, a comprehensive investigation to map the entire crack tip temperature fields has been undertaken using a 2D high speed IR camera, recently developed at Caltech. Full field thermal images of

plastic zone evolution are first presented. Subsequently, the measured temperatures are used to estimate the evolution of the J integral and the issues related to J dominant stress–strain fields within the plastic zones are discussed.

2. Experiments

2.1. Material

Temperature rise at the crack tip and within the plastic zone was investigated in two steels, featuring very different mechanical properties. One of them was C300 maraging steel, which is an ultra high strength martensitic steel, with yield stress of about 2 GPa. Its chemical composition is shown in Table 1. The specimens were cut from a plate 6.5 mm in thickness, and the heat treatment involved age hardening, by holding them at 482°C for 5 h, followed by air cooling. The mechanical properties of the age hardened C300 maraging steel can be found in Zhou et al. [14]. The mode I fracture toughness of C300 steel is about 88 MPa $m^{1/2}$. In opening mode, these specimens undergo flat fracture over most of the specimen thickness, with thin shear lips ($\sim$1 mm) on either side. The flat fracture region shows void growth and coalescence. The other steel is a highly ductile, medium strength, HY100 steel, the chemical composition of which is shown in Table 2. Its static yield strength is 800 MPa. The heat treatment involved holding at 900°C for 16 min followed by water quenching. The steel was then tempered by holding at 638°C for 50 min. As will be shown later, HY100 has very high fracture toughness and does not satisfy small scale yielding conditions in the specimen geometry used in this investigation. The typical mode I fracture surface consists of a small triangular tunneled area ahead of the crack tip, which soon gives way to shear lips covering the entire thickness. A discussion of the ductile fracture mechanisms in HY100 steel can be found in Venkert et al. [15]. HY100 displays substantial rate sensitivity, with an increase of about 20% in yield stress at a strain rate of 3000 s^{-1} compared to its value at a rate of 0.01 s^{-1}. A detailed constitutive description of HY100 steel can be found in Zhuang and Ravichandran [16].

2.2. Experimental technique

2.2.1. Infrared imaging

Discrete IR measurements has been used for measuring temperature rise in dynamic deformation and failure experiments by many investigators in the past [11,17–28]. All investigations conducted so far have utilized either a single element detector or a linear array of detectors with 8–16 sensing elements. Using a linear array of detectors, it is possible to measure temperature at a series of discrete points along a line on the specimen surface. Such detectors have been successfully used by Zehnder and Rosakis [21] and by

Table 1
Chemical composition (wt.%) of C300 maraging steel

Ni	Co	Mo	Ti	Si	Al	Cr	Cu
18.9	9.2	4.88	0.7	0.07	0.11	0.18	0.14

Table 2
Chemical composition (wt.%) of HY100 maraging steel

C	Mn	Cu	Si	Ni	Cr	Sn	Mo
0.17	0.3	0.13	0.22	2.35	1.32	0.013	0.25

Mason and Rosakis [23] to measure the temperature rise across a propagating opening crack in a high strength steel. Costin et al. [18], Hartley et al. [19], Marchand and Duffy [20], Zhou et al. [26] used them to measure the temperature rise across a propagating shear band in steels. However, the linear arrays of detectors are ideal to measure temperature distribution across features that are essentially 1D and steady. Although a great deal of information can be obtained with these linear arrays, given the highly transient 2D nature of most dynamic events in solids, including the crack tip temperature fields, it is desirable to have an instrument that can measure temperature fields over an area instead of at discrete points along a line. Since several events involving dynamic deformation in solids occur at time scales of tens of microseconds, such measurements can be accomplished using a 2D array of fast response IR detectors acquiring images at rates of around 1 MHz.

Although there have been great advances in 2D, quasi-static, IR imagery in recent years, there are currently no commercial systems capable of imaging at such high speeds. Available IR imaging systems typically run at television rates, 30 Hz, although higher speed systems do exist, with rates of up to 34 kHz. Achieving the required framing rates of up to 1MHz necessitates very fast and temporally frozen data acquisition in conjunction with a high-speed 2D IR detector array. The bottleneck in performing such measurements has been data acquisition. However, utilizing the fast, relatively inexpensive digitizers which are now available, a 2D IR imaging system has been designed and built at Caltech. This instrument, for the first time, enables the measurement of transient thermal fields at rates of up to 1 million frames per second. The complete imaging system, consisting of the focusing optics, an IR focal plane array, multiplexing circuits, and data acquisition boards is shown in the block diagram of Fig. 1. At the heart of the system is

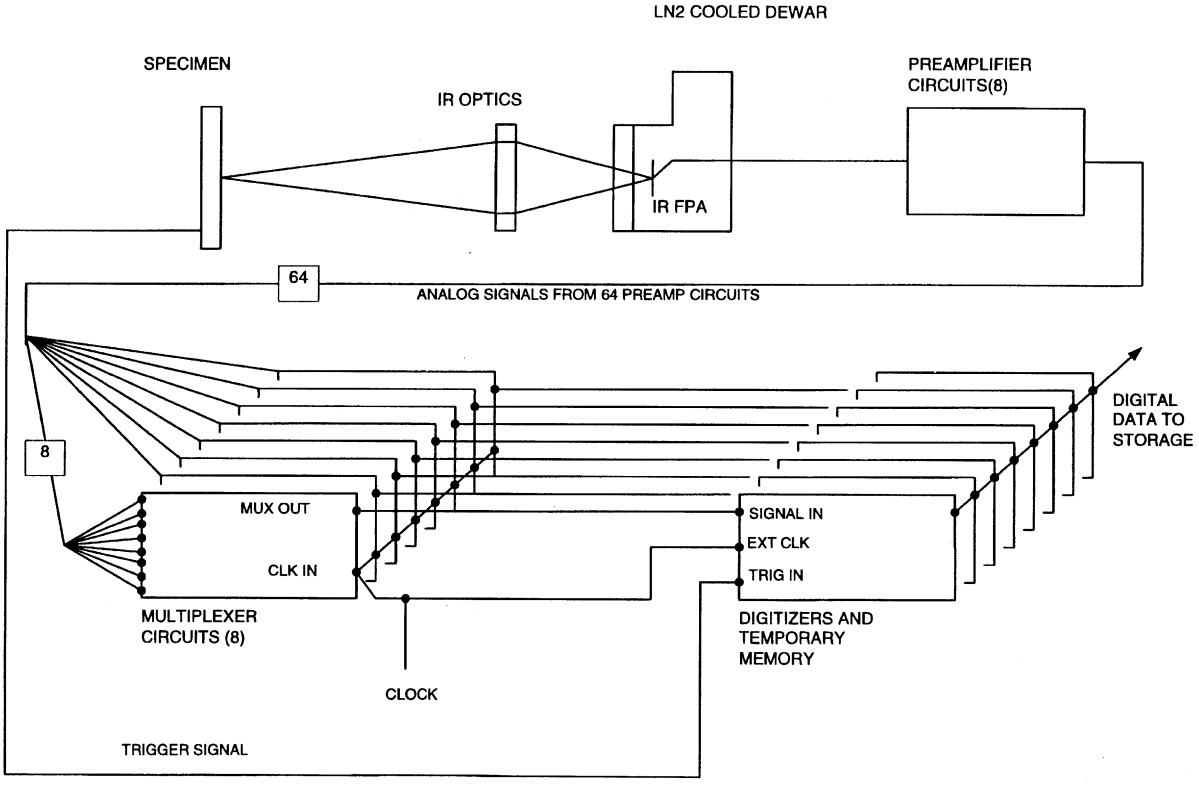

Fig. 1. Block diagram for the IR imaging system.

an 8×8 focal plane array of HgCdTe IR detector elements. Each detector element is 100 μm × 100 μm, with center to center spacing of 130 μm. Each of the 64 elements has its own preamplifier, the outputs of which are fed into a bank of eight 8:1 multiplexers. The multiplexed signals are then digitized using four two-channel, Gage 1012 A/D boards, running at speeds up to 10 MHz. Radiation emitted from the object as it deforms and heats up is focused onto the IR focal plane array using a reflective lens, built up out of two Schwarzchild objectives, each operating at infinite conjugation ratio. The ray diagram for the focusing optics is shown Fig. 2. A photograph of the camera consisting of the focusing optics and the liquid nitrogen dewar housing the detectors, is shown in Fig. 3. The magnification of each lens is fixed. To achieve different magnifications, different lenses are used. In the current investigation, a magnification of 0.9 was used to investigate the crack tip temperature field in C300 steel and a magnification of 0.48 for HY100 steel. The choice of magnification is governed by the size of the area that needs to be imaged at a specific resolution, which in turn is related to the size of the plastic zone in each case. For C300, the size of the plastic zone at crack initiation is less than 1 mm and at a magnification of 0.9, the IR camera would image an area of 1.1×1.1 mm^2. In such a case, each detector measures average temperature over an area of 110×110 μm^2. For HY100, the size of the plastic zone at initiation is around 10 mm, which is too large for the lens systems designed for the camera. Instead, it was decided to observe an area of 2.1×2.1 mm^2 close to the crack tip using a magnification of 0.48. At this magnification, each detector averages temperature over an area of 210×210 μm^2. In this system, there is no integration of the signal between frames as in commercial IR

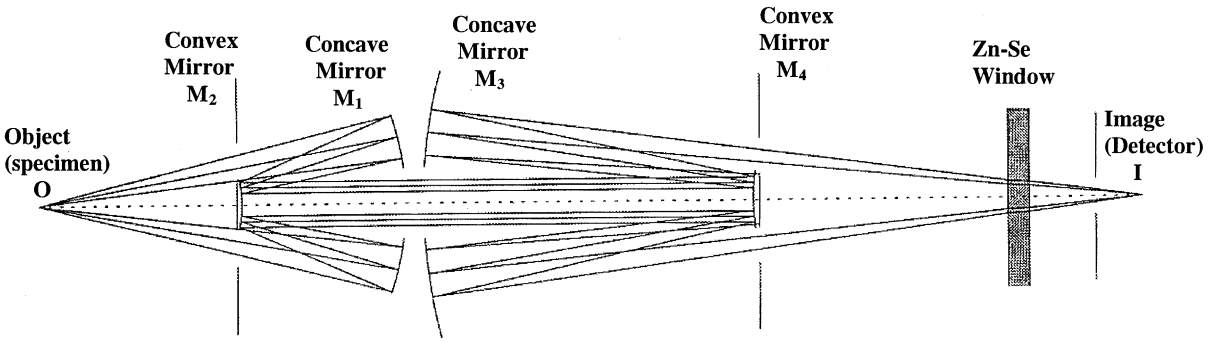

Fig. 2. Ray diagram for the double Schwarzchild focusing system.

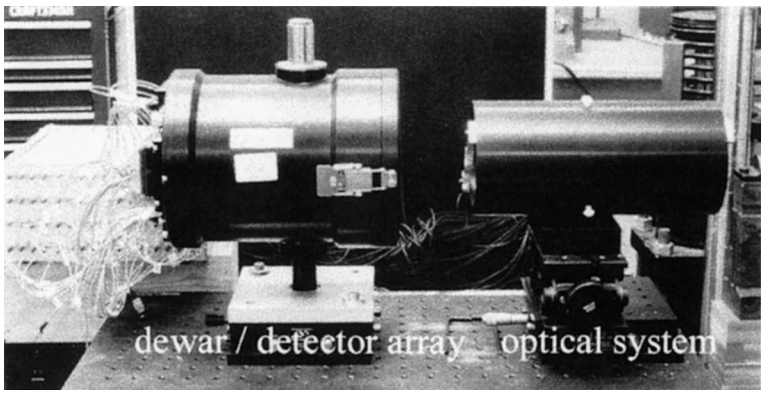

Fig. 3. A photograph of the IR imaging system.

cameras; thermal resolution is sacrificed in favor of speed. The detector response time is about 20 ns and the system rise time is approximately 750 ns. The details of each of the components of the system and the results of some preliminary applications of the system are given in Zehnder et al. [29].

2.2.2. IR system calibration

Calibration of the system is performed in a very direct manner. A sample of the same material and surface finish as will be tested is heated in an oven by a few hundred degrees. The heated sample, instrumented with a thermocouple to record its surface temperature, is placed in the object position. As the sample cools, the voltage output from each of the IR elements is recorded by the data acquisition system along with the sample temperature. This procedure provides a voltage vs. temperature curve for each element. Since the IR system is AC coupled, the input radiation to the detectors must contain an AC component. This is achieved by placing a chopping wheel in front of the heated calibration specimen. The specimen was heated repeatedly to 225°C and the calibration curves obtained for one particular detector are shown in Fig. 4.

2.3. Specimen geometry and loading arrangement

2.3.1. C300 maraging steel

The specimen geometry and loading arrangement are schematically illustrated in Fig. 5. The specimen was loaded in a three-point bend configuration under a drop weight tower (Dynatup 8100A), with a tup mass of 250 kg. The impact speed was 3 m/s. A notch, 260 μm wide and 25.4 mm long, was cut on the edge using electric discharge machining (EDM). The notch was subsequently extended by 2 mm by fatigue loading, in order to produce a sharp crack. Temperature rise during the deformation was measured in a small area of 1.1×1.1 mm^2 around the crack tip, as shown in Fig. 5. A photograph of the experimental arrangement consisting of the drop weight tower, the specimen, IR camera, amplifier bank and the data acquisition system, is shown in Fig. 6.

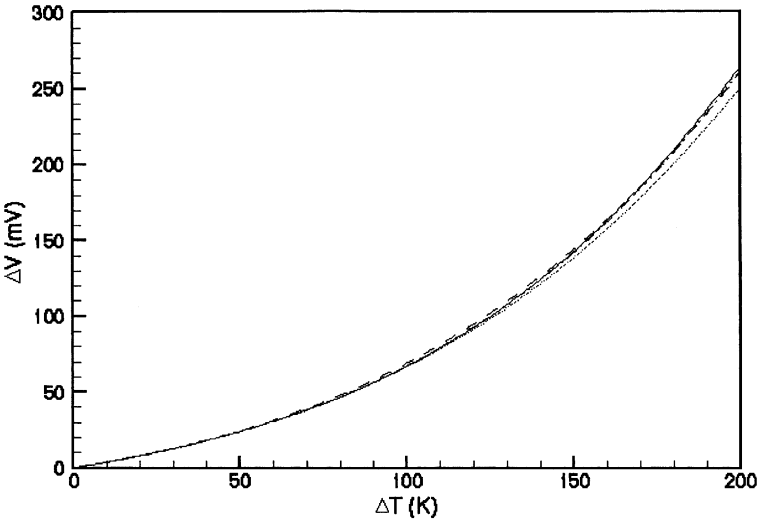

Fig. 4. Calibration curve obtained by repeatedly heating the sample to 225°C.

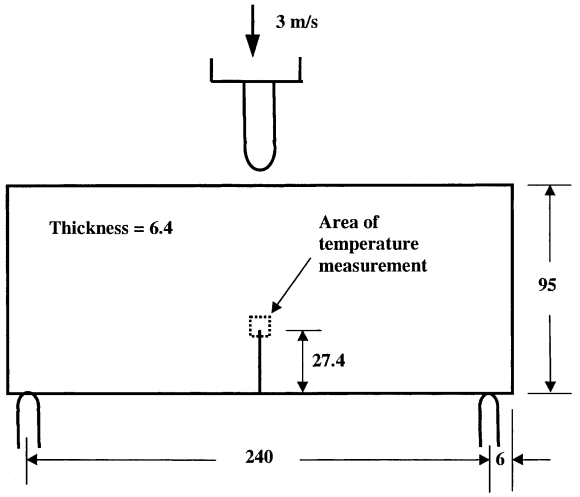

Fig. 5. A schematic illustration of the specimen geometry and loading arrangement for C300 specimens. All dimensions shown are in millimeters.

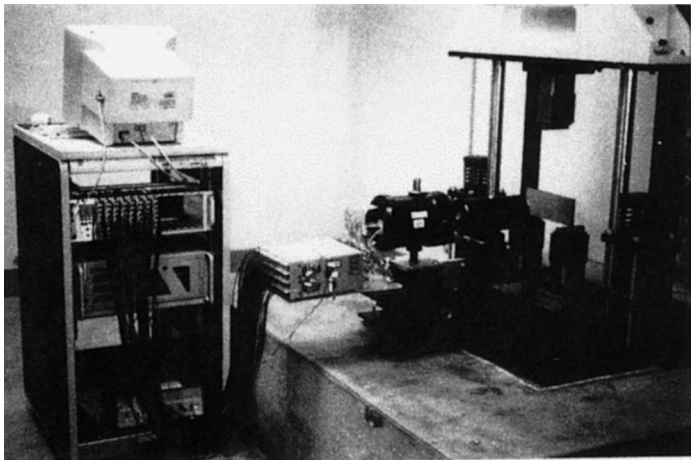

Fig. 6. A photograph of the experimental setup for testing C300 specimens under a drop weight tower.

2.3.2. HY100 steel

Loading HY100 specimens in a simple three-point bend configuration as in the case of C300 steel, presents certain experimental difficulties for temperature measurement. In a three-point bend arrangement, as the tup tries to bend the specimen, the crack tip translates downwards at about half the speed of the tup, i.e., 1.5 m/s in the C300 steel experiment. As a result, each detector on the IR camera measures temperature, not at a single targeted point on the specimen, but at several different points as they translate past the field of view of the detectors. This would not be a major problem if the total translation prior to crack initiation were small compared to the size of the field of view of the camera. For example, in the case of C300 steel, crack initiates around 200 μs, during which time, the crack tip travels about 300 μm downwards, which is small compared to the size of the field of view. However, since, HY100 steel is much more ductile, crack

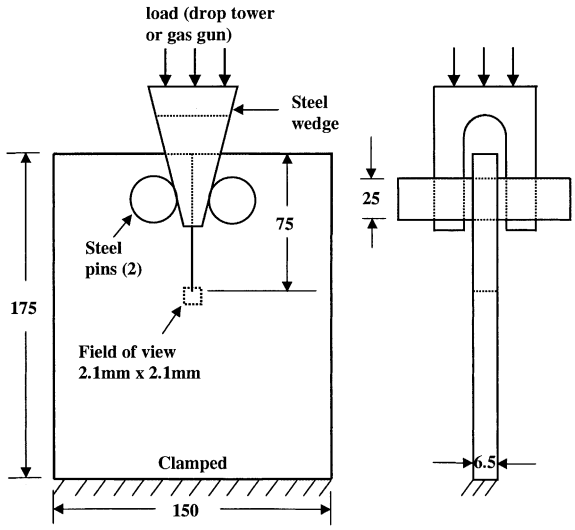

Fig. 7. A schematic illustration of the specimen geometry and loading arrangement for HY100 specimens. All dimensions shown are in millimeters.

initiation takes place after a substantially larger translation, compared to the size of the field of view. Thus, in order to load the specimen in mode I, without any crack tip translation, a specimen geometry was designed as shown in Fig. 7. This is a modification of the geometry used by Zehnder and Rosakis [21]. The loading is produced by driving a wedge which separates two pins that open the crack in mode I. The bottom of the specimen is securely clamped to a rigid base in order to prevent any translation. The load to drive the wedge is provided by placing the specimen-wedge assembly under a drop weight tower or impacting the wedge with a projectile accelerated in a gas gun. For HY100 steel, two loading rates were used. First, the specimens were subjected to drop weight impact at a speed of 4 m/s. To achieve a higher rate of loading, it was subjected to a 50 m/s projectile impact. The cylindrical steel projectile used was 50 mm in diameter and 127 mm long. A schematic of the latter experimental arrangement for gas gun impact is shown in Fig. 8.

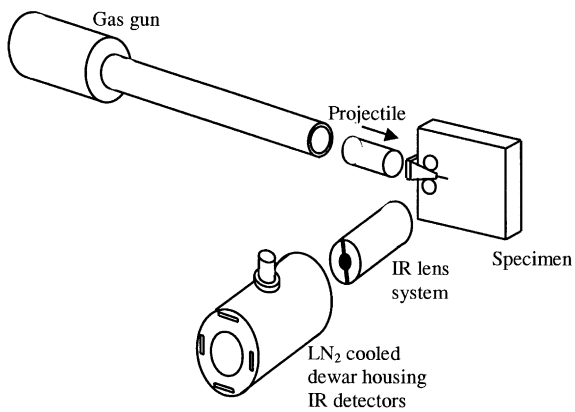

Fig. 8. A schematic illustration of the experimental setup for testing HY100 specimens with a gas gun and measure the crack tip temperature field.

3. Results

3.1. C300 steel

3.1.1. Temperature images

Two sequences of thermal images, showing the initiation and propagation of the crack, respectively, are shown in Figs. 9 and 10. It should be recalled that the temperature field is measured at 64 discrete points. The images shown are the projections on the x_1–x_2 plane of the contour lines on a surface fitted through the 64 points in the x_1–x_2–ΔT (temperature rise) space. In Fig. 9, starting about 170 μs after impact, a plastic zone can be seen building up. A black line is artificially superimposed on these images to indicate the approximate location of the crack. The position of the crack is inferred from the temperature patterns. The black line is not shown beyond 210 μs because, beyond this time, the position of the crack tip is presumed to have moved outside the field of view due to the specimen translation described in Section 2.3.2. In spite of some initial asymmetry, the plastic zone builds up almost symmetrically and gradually up to 226 μs. The first image in Fig. 10 is the same as the last one in Fig. 9, shown at a different temperature scale. Beyond 226 μs, an asymmetry in temperature distribution can be seen to build rapidly, which is the result of the process of crack growth. The red band of high temperatures in the latter images of Fig. 10 is actually the intersection of the shear lip with the free surface. The temperatures at the center of the band reach as high as

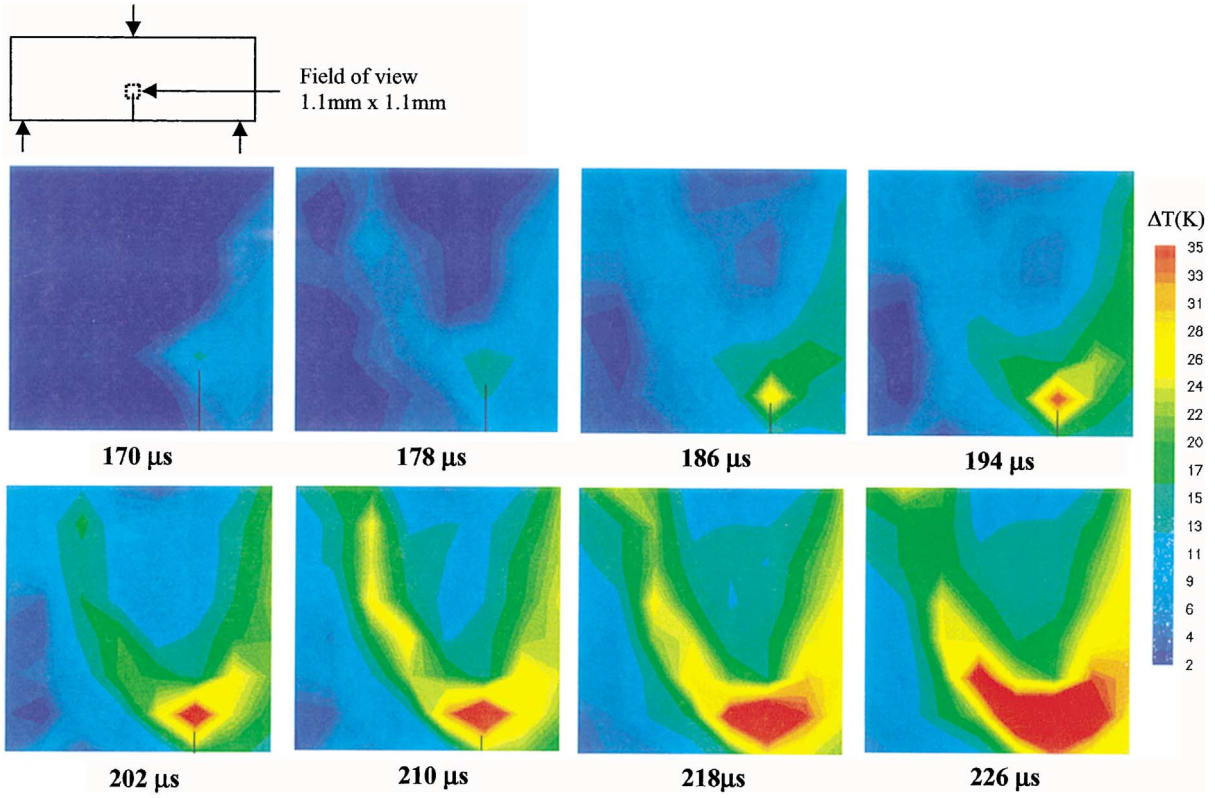

Fig. 9. A sequence of thermal images showing the development of the plastic zone until initiation. The black line is the assumed crack location. The images capture the development of temperature field within the plastic zone.

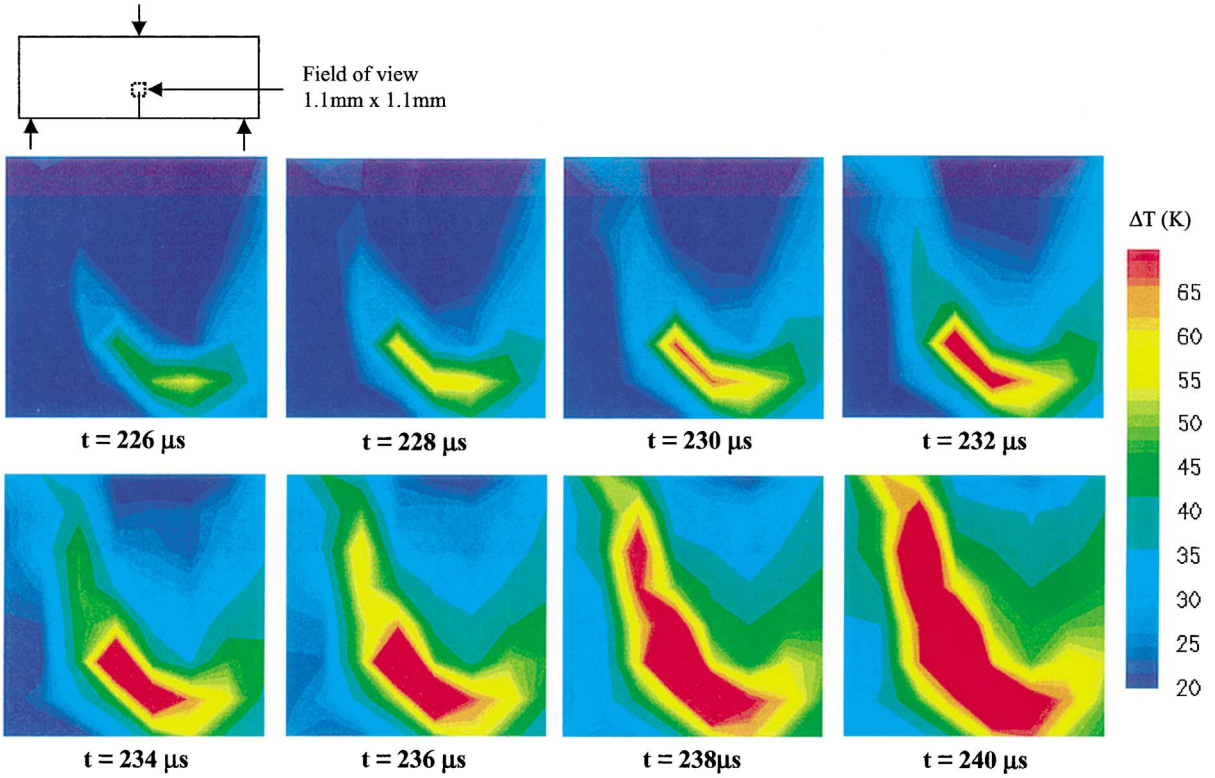

Fig. 10. A sequence of images showing the development of the temperature field for a just initiated crack. The high temperature imaged is a result of material fracture.

200°C. A detailed image of the propagating crack is shown in Fig. 11. This is the first time that such images showing the process of crack initiation and propagation, detailing the shape and growth of the plastic zone and its temperature structure within, in real time, have been obtained. From Figs. 9 and 10, it can be concluded that 226 μs is the time of crack initiation and that the maximum temperature rise at the crack tip at initiation is around 55°C. However, each IR detector averages temperature over an area of 110×110 μm^2. Since the temperature gradients are expected to be high near the crack tip, the maximum local temperature could actually be higher than 55°C.

3.1.2. Comparison with the Rice and Levy model

Rice and Levy [3] (RL) modeled the temperature rise at the tip of a stationary crack for small scale yielding, using the plane strain slip line analysis and the J integral. The slip line analysis gives the rate of plastic dissipation within the plastic zone to be

$$\dot{W}^{\mathrm{p}} = \frac{\tau_0^2}{\mu r} \cos 2\left(\theta - \frac{\pi}{2}\right)\dot{\omega} \tag{1}$$

where τ_0 is the shear yield stress, μ is the shear modulus, (r, θ) are the crack tip polar coordinates, with $\theta = 0$ denoting the crack line ahead of the tip and ω is the maximum extent of the plastic zone, which is given by

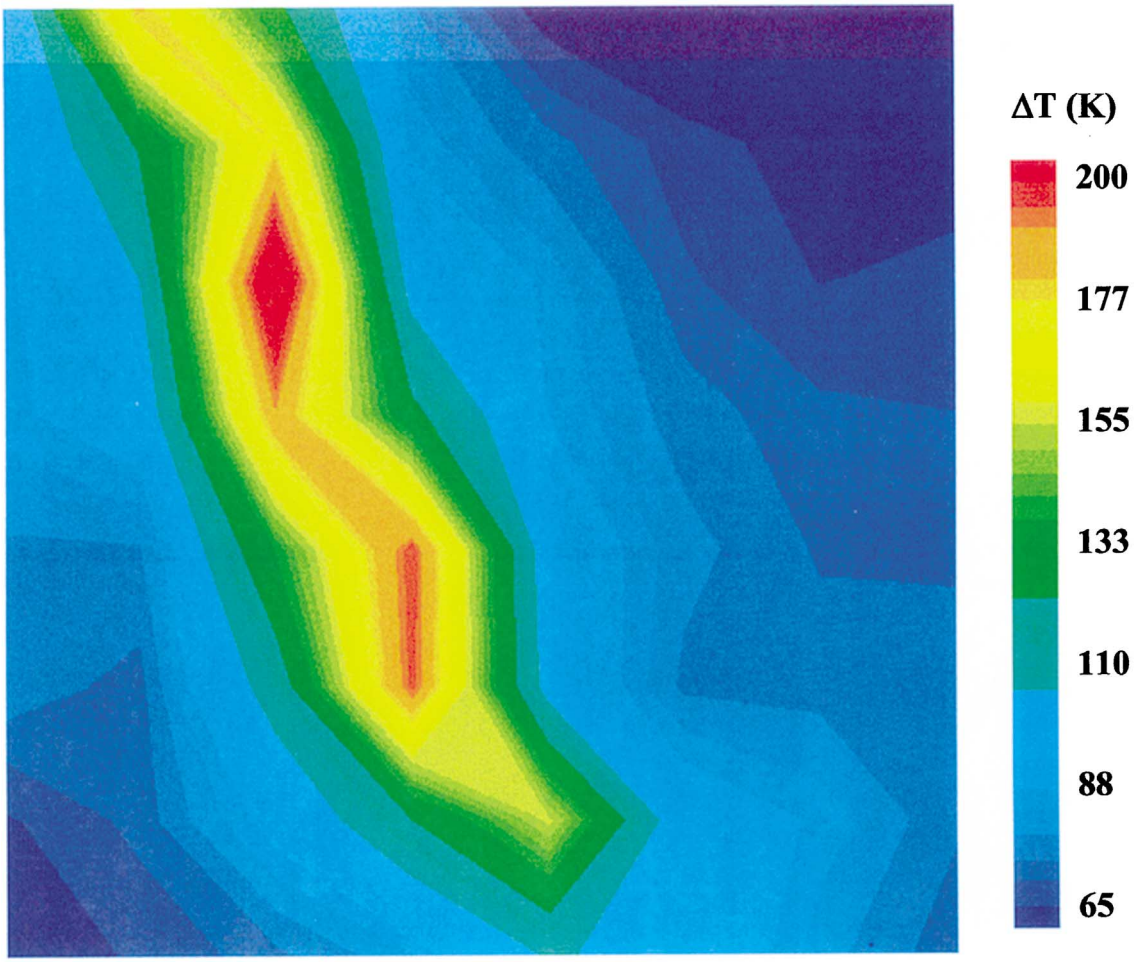

Fig. 11. A detailed image of temperature distribution near a propagating crack.

$$\omega = \frac{3(1-\nu)}{\sqrt{2}(2+\pi)}\left(\frac{K}{2\tau_0}\right)^2 \tag{2}$$

where ν is the Poisson's ratio and K is the far field stress intensity factor. Before considering the complete heat conduction analysis of RL, let us first assume adiabatic conditions and estimate the temperature rise. For adiabatic conditions, Eq. (1) can be integrated directly. Using Eq. (2) and by assuming that all of plastic work is converted into heat, the temperature rise near the crack tip at initiation can be estimated to be

$$\Delta T = \frac{2.23}{r} \tag{3}$$

where r is in millimeters and ΔT is in °C. The following values have been used in the above calculation. $K = 88$ MPa $\mathrm{m}^{1/2}$; $\tau_0 = 1$ GPa; $\mu = 70$ GPa; $\nu = 0.3$; $\rho = 8000$ kg/m^3; $c = 450$ J/kg/K; and $\theta = \pi/2$ for an upper bound estimate. Since each IR detector averages temperature over a spot of 110 μm × 110 μm, it would be appropriate to compare the measured crack tip temperature with an estimate from Eq. (3), using

$r = 55$ μm, which yields $\Delta T = 41$°C. This compares very well with the measured value of 55°C. However, as RL pointed out, since the temperature distribution according to this analysis has a $1/r$ singularity, the crack tip would never be under truly adiabatic conditions. RL solved the heat conduction problem for the crack tip temperature rise, by considering the heat generated over the entire plastic zone for the plane strain slip line model. The solution is given below.

$$\Delta T = \left(0.156\frac{(1-\nu^2)K^2}{E\sqrt{\rho c k \tau}}\right)h(\delta) \tag{4}$$

where τ is the time for the stress intensity factor to increase from 0 to its critical value of 88 MPa $m^{1/2}$, which is about 200 μs in this case. k is the coefficient of thermal conduction, 36 W/m/K. $h(\delta)$ is a dimensionless function of the dimensionless parameter δ which is a measure of the shortness of the time to reach the maximum stress intensity factor and is defined as $\delta = 2\sqrt{\alpha\tau}/\omega$, where α is the thermal diffusivity, 10^{-5} m^2/s. For the values listed above, $\delta = 0.16$, for which $h(\delta)$ is 0.85 from Ref. [3]. Using these values in Eq. (4), the crack tip temperature rise is estimated to be approximately 30°C. Though RL model predicts the crack tip temperature to the correct order, it is an underestimation of the actual value of 55°C. The discrepancy can be attributed to the assumptions made in using the model for the present case. The model was developed for the case of plane strain, which is not a valid state at the specimen free surface, where the conditions are closer to plane stress. For a given stress intensity factor, the strains are higher for plane stress, leading to higher temperatures as observed in the experiment. The crack tip finite strains could be another factor, which are not considered in the RL model. Away from the crack tip, adiabatic conditions are expected to be a better approximation. Hence, the adiabatic model discussed above can be used to predict the temperature rise there. According to Eq. (3), the temperature rise falls rapidly to about 2°C at a distance of 1 mm from the crack tip. This seems to agree very well with the experiment as can be discerned from the last two images of Fig. 9.

It is generally known that when a specimen is subjected to mode I loading, the conditions at the free surface would be close to a plane stress situation and the conditions at the mid-plane would be close to a plane strain situation. Thus it was surprising to find the temperature contours at the specimen surface, as observed by the IR camera, have a characteristic U shape near the crack tip, whereas, such a shape is typically associated with a plane strain plastic zone. An explanation for this can be found from the 3D numerical investigations of the shapes of the plastic zones of statically loaded three-point bend 4340 steel specimens, by Narasimhan and Rosakis (NR) [30]. 3D numerical simulations of thin metal plates were also conducted by Nakamura and Parks [31] and similar results were reported. The numerical simulations revealed that the contours of equivalent stress within the plastic zone, at the free surface, actually show a characteristic U shape that was observed in the experiments. A qualitative comparison of the results of NR with the current experiment is shown in Fig. 12. Fig. 12a is a thermal image at the time of crack initiation and Fig. 12b shows the contours of equivalent stress within the plastic zone for a 10 mm thick 4340 steel plate, with a yield stress of 1030 MPa and loaded to a stress intensity factor of 280 MPa $m^{1/2}$. The figure also shows the corresponding adiabatic temperature rise values along the contours, which were not originally reported by NR, but were calculated here for the purpose of comparison. Using J_2 incremental plasticity and linear-power law relation between stress and strain, a straight forward calculation results in the following relation between the temperature rise (ΔT) and the equivalent stress (σ_e).

$$\Delta T = \frac{1}{\rho c}\left[\frac{n}{n+1}\frac{\varepsilon_0}{\sigma_0^n}\sigma_e^{n+1} - \frac{\varepsilon_0}{2\sigma_0}\sigma_e^2\right] \tag{5}$$

where, ρ is the material density, c is the specific heat, n is the hardening exponent, σ_0 is the yield stress and ε_0 is the yield strain. Given the difference in the material properties, loading conditions and the experimental geometry, it is not possible to make a direct quantitative comparison between Fig. 12a and b. However, two observations can be made. The equivalent stress contours indeed show the characteristic U shape near the

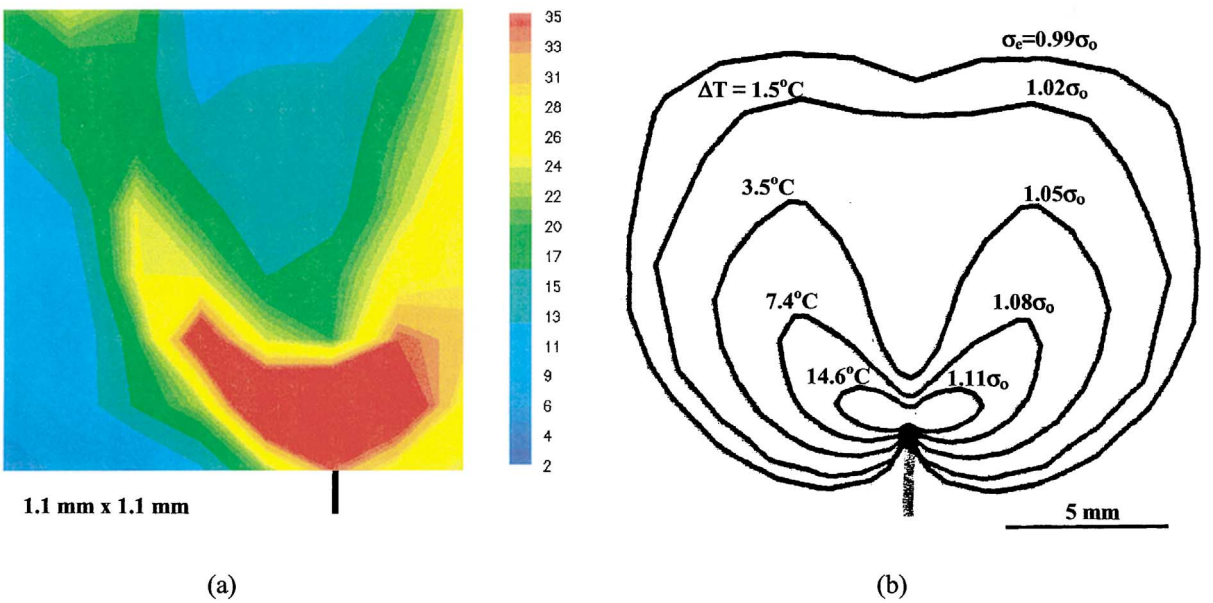

Fig. 12. (a) A thermal image of crack tip region in C300 at initiation. (b) The plastic zone with the contours of equivalent stress and the corresponding temperature rise for a 4340 steel, from the numerical simulations of Narasimhan and Rosakis [30].

crack tip, which is supported by the experiments. Such a shape is a consequence of the presence of the free boundary. In the numerical simulation, the applied K is almost three times that in the experiment and the yield stress is only one-half of that of C300 steel. Hence, crack tip plastic zone length scale is approximately 36 times bigger in the simulation compared to that in the current experiment, which accounts for the big difference in size between Fig. 12a and b. This difference in length scale also provides a way to compare the two pictures appropriately, by scaling down Fig. 12b by the factor 36. Thus the plastic zone shown in Fig. 12b is about 600×600 μm^2 when scaled down, and the temperature contour values are indeed within the order of magnitude of the measured values.

3.2. HY100 steel

3.2.1. Temperature images

A sequence of thermal images obtained in the drop weight tower experiment with an impact speed of 4 m/s is shown in Fig. 13. A plastic zone can be seen growing beginning at 950 μs. The peak temperatures observed are significantly higher than those observed in C300 steel. The maximum temperature at the crack tip in the last image is around 90°C. This is not unexpected because of the extensive plastic deformation that HY100 steel can sustain prior to failure. Once again, the familiar U shaped temperature rise contours close the crack tip can be observed. One of the persistent difficulties in the study of the dynamic fracture of ductile metals has been the reliable identification of crack initiation time. In the past a variety of techniques have been used to identify crack initiation with varying degree of success. In the current investigation, the following procedure has been followed to identify crack initiation. Fig. 14b shows the temperature signals for five individual detectors, located along a line ahead of the crack, as shown schematically in Fig. 14a, for the drop weight tower experiment. The area shown in Fig. 14a is the field of view of the IR camera and the digits denote the individual detectors along the column that is directly ahead of the crack tip. The temperature signals increase steadily at the beginning and at around 1600 μs, show a marked increase in slope.

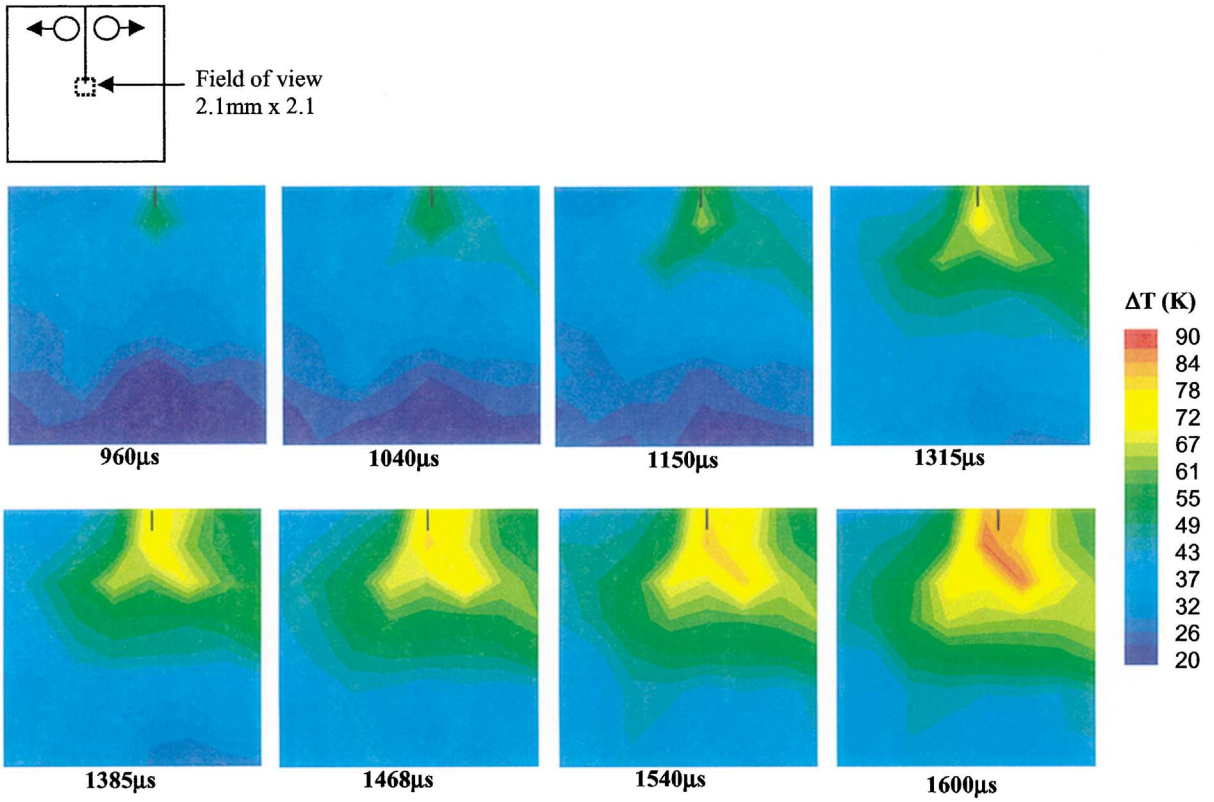

Fig. 13. A sequence of images showing the evolution of the temperature field at the crack tip in a HY100 specimen subjected to drop weight impact at 4 m/s.

This increase in slope can be associated with crack initiation in the form of tunneling at the center of the specimen. Initially when the crack tip is loaded, the region in front of the crack tip throughout the specimen thickness is plastically deformed and the temperature increases. However, when crack initiation begins in the form of tunneling at the center plane of the specimen, subsequent deformation gets concentrated in the two ligaments on either side of the tunnel. Thus the rate of plastic deformation on the specimen surface in front of the crack tip increases following tunneling, resulting in an increase in the slope of the temperature signals seen in Fig. 14b. From this figure, the crack initiation event can be identified to be at 1600 μs.

A sequence of images, obtained from the gas gun experiment with an impact speed of 50 m/s is shown in Fig. 15. As before, failure initiation can be identified to be around 140 μs, from Fig. 16a and b. Failure occurs an order of magnitude faster here compared to the drop weight tower experiment. The small flat portion of the temperature signals following initiation suggests the highly dynamic nature of the initiation event, resulting in momentary unloading before further plastic deformation. One major difference between the two experiments is the maximum crack tip temperature rise at the time of initiation. It is approximately 90 K in the drop weight experiment and about 150 K in the gas gun experiment. The explanation for this lies in the rate induced elevation of resistance to crack initiation. To investigate this issue further, the measured temperature signals were used to estimate the evolution of an appropriate fracture parameter. Following Guduru et al. [11], it was assumed that the HRR stress–strain field characterized by the J integral exists around the crack tip area and the measured temperatures were used to estimate the evolution of the J integral and its critical value at initiation.

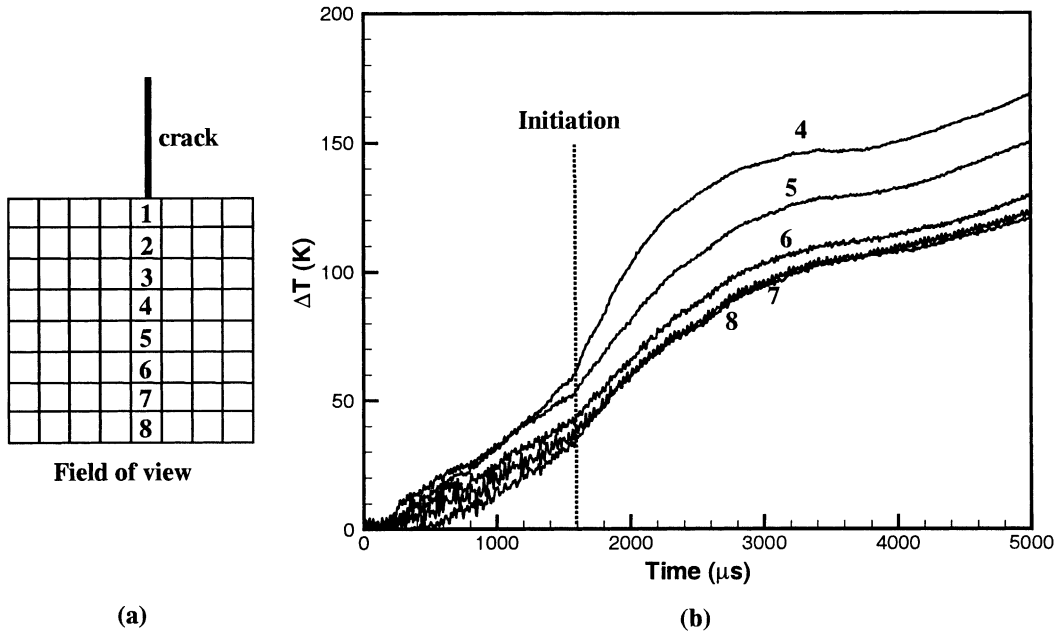

Fig. 14. (a) Schematic illustration of the area of temperature measurement and the position of the crack tip. The digits represent the detectors focused along the crack line. (b) Temperature signals from the detectors on the crack line.

3.2.2. J integral estimation

3.2.2.1. Asymptotic stress field: Hutchinson [12] and Rice and Rosengren [13], considered the case of a monotonically loaded stationary crack in a material described by a J_2-deformation theory of plasticity and a power hardening law. They showed that the strain and stress components in the crack tip region scale with the value of the J integral. Within the small strain assumption, an asymptotic solution of the elastic–plastic field equations in the crack tip region has the form

$$\varepsilon_{ij} = \varepsilon_0 \left[\frac{J}{\sigma_0 \varepsilon_0 I_n r} \right]^{\frac{n}{n+1}} E_{ij}(n, \theta) \tag{6}$$

$$\sigma_{ij} = \sigma_0 \left[\frac{J}{\sigma_0 \varepsilon_0 I_n r} \right]^{\frac{1}{n+1}} \Sigma_{ij}(n, \theta) \tag{7}$$

Here, σ_0 is the tensile yield stress, ε_0 is the equivalent tensile yield strain, n is the hardening exponent, and the angular factors Σ_{ij} and E_{ij} depend on the mode of loading and the hardening exponent. The dimensionless quantity I_n was defined by Hutchinson [12].

3.2.2.2. Temperature rise associated with the HRR singular field: Consider an elastic–plastic isotropic homogeneous material with constant thermal conductivity. The heat conduction equation can be written as [32]

$$k\nabla^2 T - \eta(3\lambda + 2\mu) T_0 \dot{\varepsilon}^{\mathrm{e}}_{kk} + \beta \sigma_{ij} \dot{\varepsilon}^{\mathrm{p}}_{ij} = \rho c \dot{T} \tag{8}$$

where k is the thermal conductivity, T the absolute temperature, η the coefficient of thermal expansion, λ and μ Lame constants, T_0 the initial temperature, ε_{ij} and σ_{ij} the Cartesian components of the strain and

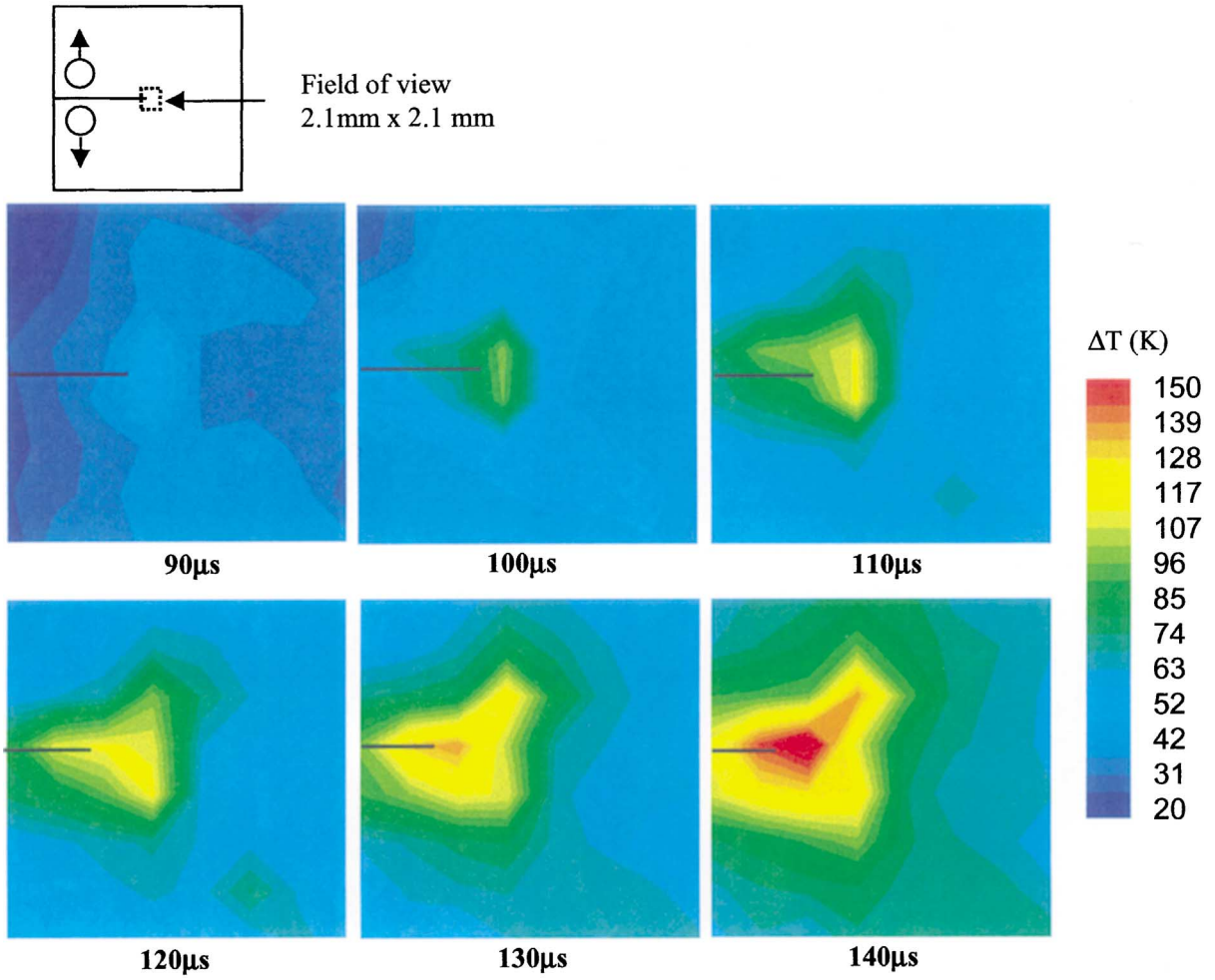

Fig. 15. A sequence of images showing the evolution of the temperature field at the crack tip in a HY100 specimen subjected to gas gun impact at 50 m/s.

stress tensors, respectively. Superscripts 'e' and 'p' stand for the elastic and the plastic components, respectively. ρ is the mass density and c is the specific heat. β is the fraction of plastic work density rate $\dot{W}^{\mathrm{p}} = \sigma_{ij}\dot{\varepsilon}^{\mathrm{p}}_{ij}$, dissipated as heat. Assuming that the elastic strain components are small compared to the plastic strain components, the thermoelastic term in the above equation can be neglected. If the process is assumed to be adiabatic, the above equation reduces to

$$\frac{\beta}{\rho c}\sigma_{ij}\dot{\varepsilon}^{\mathrm{p}}_{ij} = \dot{T} \tag{9}$$

Substituting Eqs. (6) and (7) into Eq. (9) and integrating with time, we have

$$J(t) = \frac{\rho c I_n}{\beta}\left(\frac{n+1}{n}\right)\frac{r}{\Sigma_{ij}(\theta,n)E_{ij}(\theta,n)}\Delta T(r,\theta,t) \tag{10}$$

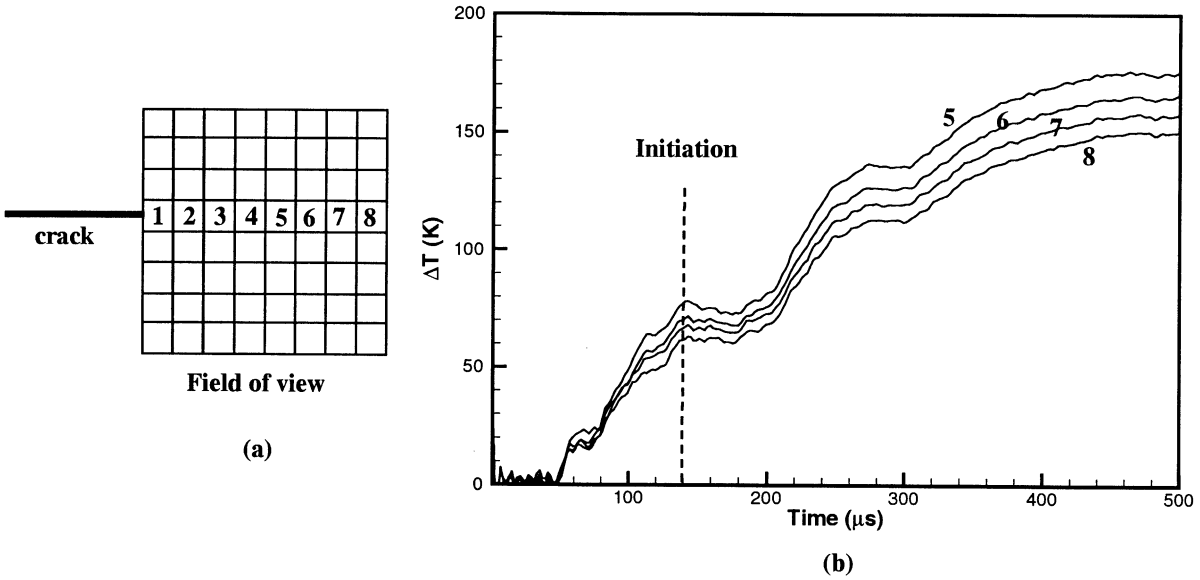

Fig. 16. (a) Schematic illustration of the area of temperature measurement and the position of the crack tip. The digits represent the detectors focussed along the crack line. (b) Temperature signals from the detectors on the crack line.

This equation provides a direct relation between the temperature rise at a point within the plastic zone and the J integral. Plane stress values of the angular functions and I_n are used, with a value of 8 for n. The value of β is assumed to be 1.0. This calculation is illustrated in Fig. 17 for the drop weight tower experiment. Using the temperature rise at points that are directly ahead of the crack tip, the J integral as calculated from

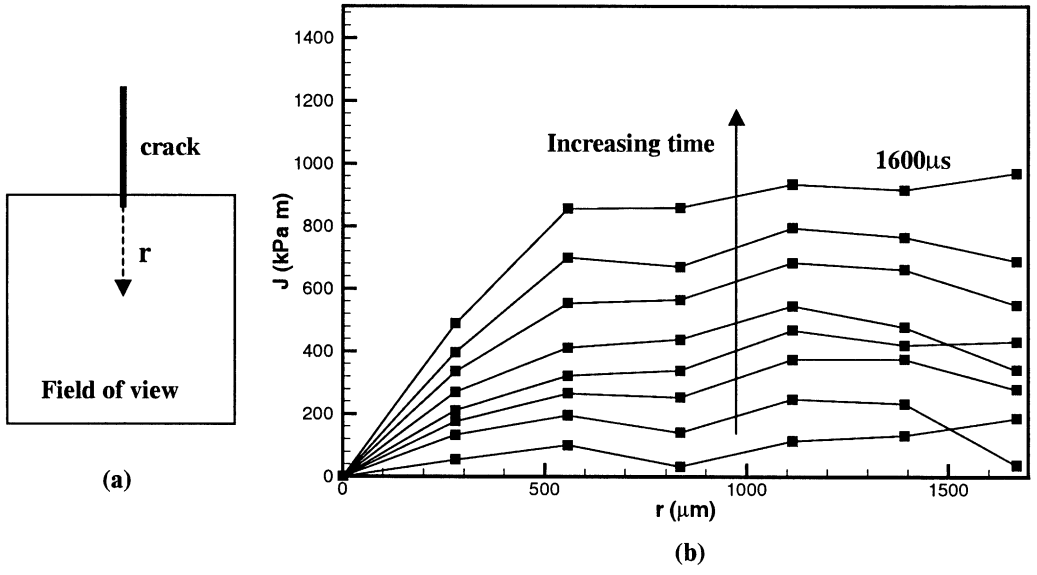

Fig. 17. (a) Schematic illustration of the area of temperature measurement with respect to the crack tip. (b) Evolution of the J integral as a function of time, as calculated from the temperature signals along the crack line for the drop weight tower impact.

Eq. (10) is plotted as a function of the distance from the crack tip, at different times, separated by 200 μs, up to crack initiation. Each line in Fig. 17 represents the calculation from Eq. (10) of J vs. r at a given time. If there were complete HRR field dominance everywhere near the crack tip, each line would be a straight horizontal line, corresponding to the value of J at that instant. The figure shows that it is almost constant beyond a certain distance from the crack tip, indicating the existence of the HRR field there. At 1600 μs, which is the approximate time of crack initiation, J has a value of about 850 kPa m. The calculation is repeated for the gas gun experiment and is shown in Fig. 18. The various lines are calculations at times separated by 20 μs and 140 μs is the crack initiation time. The critical J in this case can be deduced to be about 1225 kPa m. Note that in this case, J dominant field is not as well established as in the previous case, possibly due to inertial and rate sensitivity effects, which are not accounted for in this analysis. Note the significant increase in the critical value of the J integral at the higher loading rate. This is not surprising since the loading rate is an order of magnitude higher and the material is substantially rate sensitive [33]. These values are similar in magnitude to those reported by Guduru et al. [11] for a similar Ni–Cr steel and a stainless steel, both of which are also highly ductile. This calculation clearly demonstrates the utility of full field temperature measurements in investigating the dynamic fracture toughness characteristics of ductile metals. In order to further illustrate the HRR character of the measured temperature distribution, it is compared with the distribution predicted by the HRR field, with a chosen value of J integral to yield the best fit. These comparisons are shown, respectively, in Fig. 19 for the drop tower case at the initiation time (1600 μs) and in Fig. 20 for the gas gun case at 120 μs. In these figures, the symbols are the experimentally measured temperature rises at discrete points ahead of the crack tip and the solid line is the HRR prediction. The close agreement between the two beyond a finite distance from the crack tip indicates possible existence of the HRR field there. Close to the crack tip, the measured temperatures are lower than the HRR values, presumably because of finite area temperature averaging in the experiment and crack blunting.

It was shown by Narasimhan and Rosakis [30] that the stress field at the free surface of the specimen, within the plastic zone, follows the plane stress HRR field, which justifies the use of the plane stress fields in Eq. (9) above. It was also shown that the J integral decreases from the specimen mid-plane towards the free

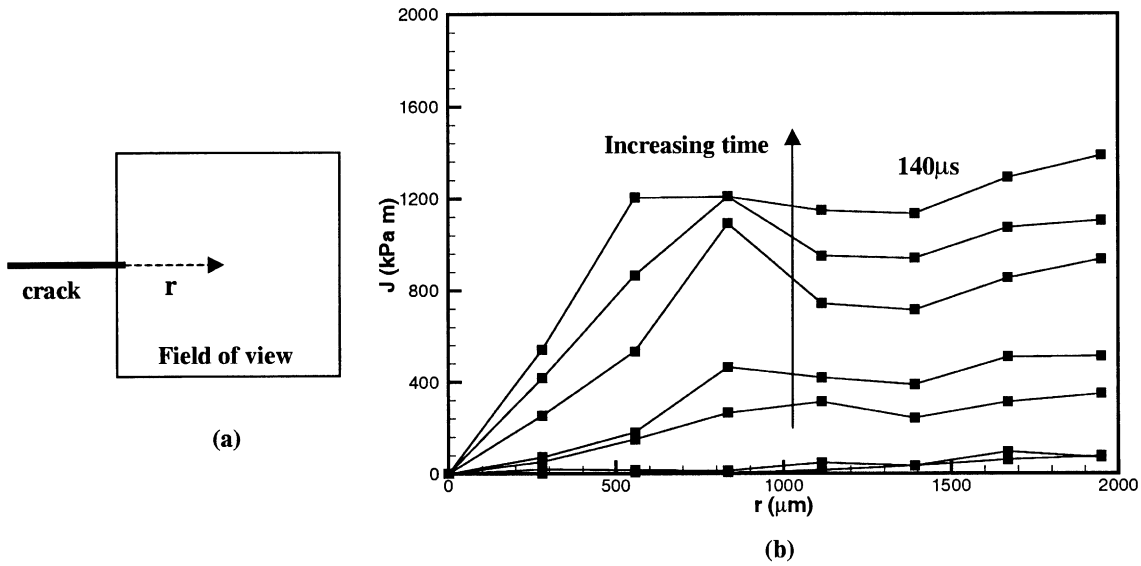

Fig. 18. (a) Schematic illustration of the area of temperature measurement with respect to the crack tip. (b) Evolution of the J integral as a function of time, as calculated from the temperature signals along the crack line for the gas gun impact.

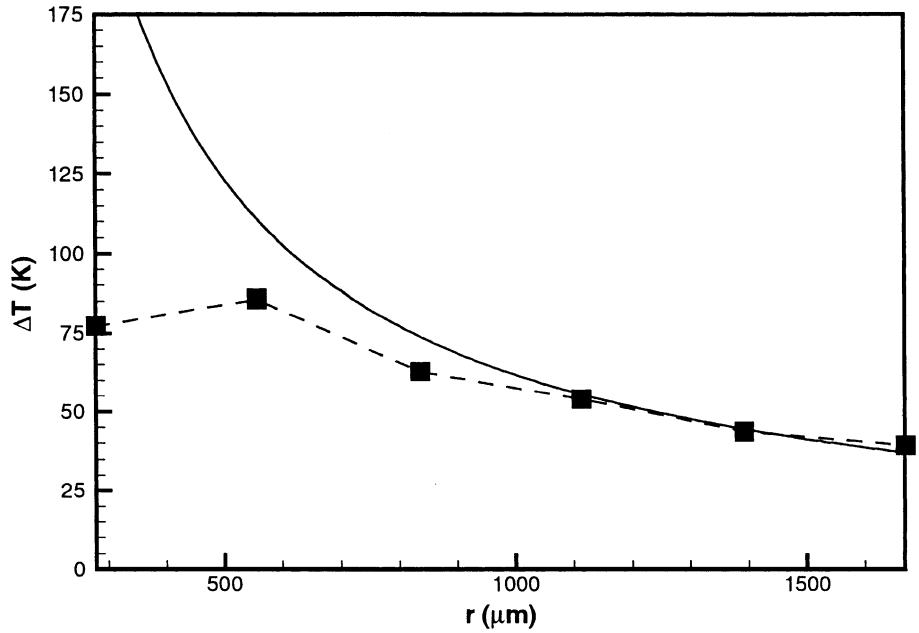

Fig. 19. An illustration of the HRR character of the temperature distribution in the drop weight tower experiment. Solid line is the HRR fit to the experimental data represented by the symbols.

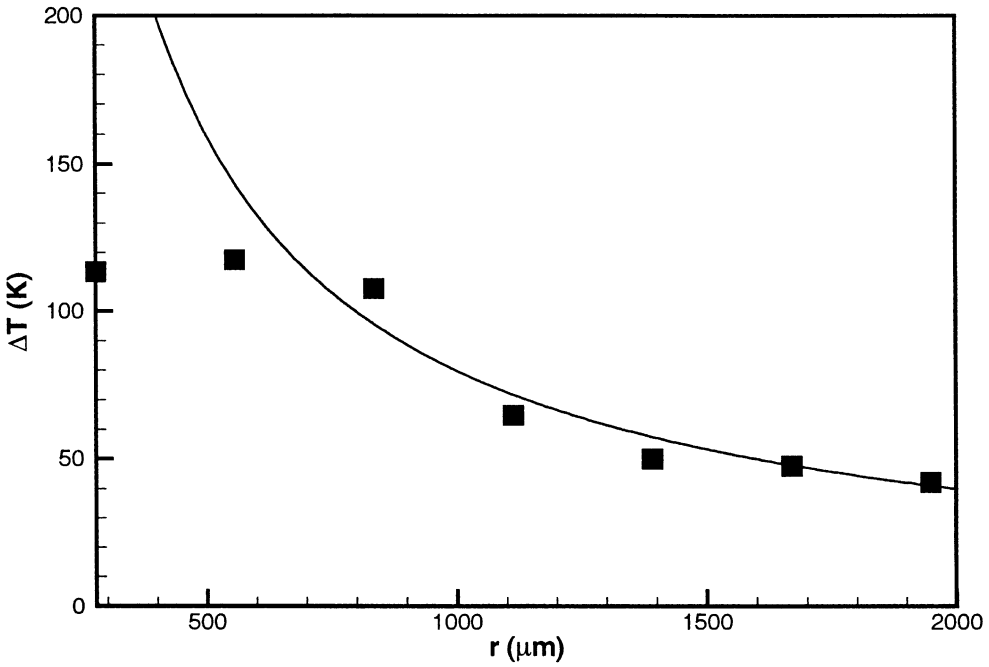

Fig. 20. An illustration of the HRR character of the temperature distribution in the gas gun experiment. Solid line is the HRR fit to the experimental data represented by the symbols.

surface. The J integral estimated from the surface temperature measurements, thus, is the surface J and thus cannot be used as a critical parameter for crack initiation in specimens of finite thickness. However, an increase in the critical surface J certainly indicates an increase in resistance to fracture. On the other hand, given the relative accuracy and convenience of IR temperature measurement, it would be desirable to develop a way to use such a measurement as a tool to compare the dynamic fracture resistance among different materials as well as to investigate the effect of loading rate on the fracture toughness for a given material. A step in that direction would be a systematic parametric numerical investigation of specimens of finite geometry to relate the surface J to the thickness averaged J, which can serve as a better fracture parameter.

4. Concluding remarks

This investigation, for the first time, captured the real time evolution of the temperature fields at the crack tips in two steels, a high strength steel and a highly ductile steel. The temperature fields recorded are at the surface of the specimen. Inside the specimen, because of the plane strain constraint, the plastic strains are expected to be lower and hence lower temperatures. The thermal images also provide an opportunity to test models and analyses that predict the temperatures at stationary cracks, the size and the shape of the plastic zone and the plastic work dissipation distribution therein. The RL model predicts the crack tip temperature to within the order of magnitude and the differences can be attributed to the fact that the model was developed for the plane strain situation. No attempt has been made to compare the RL model with temperatures in HY100 steel because there was no independent information about the value of the critical J integral other than that from temperature measurements. The HRR field, used to extract the J integral value, predicts a $1/r$ variation for the temperature rise within the plastic zone. RL model also predicts a $1/r$ variation. Using the HRR based J in the RL model to predict the temperatures will merely be an exercise in checking the closeness between the hardening (HRR) and non-hardening (RL) models. In the foregoing analysis, the existence of the HRR field within the plastic zone around the crack tip has been tacitly assumed. However, mere observation of $1/r$ temperature behavior does not prove the existence of the HRR field, even though such a field predicts $1/r$ dependence. The use of the HRR field here is guided by the past numerical and experimental work on similar structural steels and experimental geometry [30,31,34–36].

Identifying crack initiation accurately in ductile fracture has always been a gray area in determining the dynamic fracture toughness. If initiation is defined as the first coalescence of voids with the main crack near the mid-plane of the specimen, static fracture toughness can be determined by subjecting several specimens to progressively higher loads and conducting a post-test examination. Multi-specimen methods have also been used under dynamic conditions using techniques such as the stop-block technique and the low-blow test, with limited success [37]. For a single-specimen dynamic test, a variety of methods have been used in the past to infer the time of crack initiation. They include placing a strain gage close to the crack tip and looking for a change in the slope of the signal from the gage, the change in the slope of the crack opening displacement [11,38], magnetic emission detection near the crack tip [39] and constructing the "key curves" [40]. This investigation offers a temperature based procedure to identify crack initiation. However, none of the methods have been independently verified by other techniques to check their consistency and repeatability and this is an area that requires further attention.

Acknowledgements

This work was supported by the Engineering Research Program of the Office of Basic Energy Sciences at the Department of Energy through grant # DE-FG03-95ER14560 (Dr. Robert Price, Project Officer). PRG

is pleased to acknowledge many useful discussions with Dr. David M. Owen, Caltech during the course of this work.

References

[1] Freund LB. Dynamic fracture mechanics. Cambridge: Cambridge University Press; 1990.
[2] Kraft JM, Irwin GR. Crack velocity considerations. Symposium on Fracture Toughness Testing and its Applications, ASTM STP 381, Philadelphia; 1965. p. 114–29.
[3] Rice JR, Levy N. Local heating by plastic deformation at a crack tip. In: Argon AS, editor. The physics of strength and plasticity. Cambridge, MA: MIT Press; 1969. p. 277–92.
[4] Jha M, Narasimhan R. A finite element analysis of dynamic fracture initiation by ductile failure mechanisms in a 4340 steel. Int J Fracture 1992;56:209–31.
[5] Basu S, Narasimhan R. A finite element study of the effects of material characteristics and crack tip constraint on dynamic ductile fracture initiation. J Mech Phys Solids 1999;47:325–50.
[6] Wilson ML, Hawley RH, Duffy J. The effect of loading rate and temperature on fracture initiation in 1020 hot rolled steel. Engng Fracture Mech 1980;13:371–85.
[7] Rabin Y, Rittel D. A model for the time response of solid embedded thermocouples. Exp Mech 1999;39:132–6.
[8] Wells AA. The mechanics of notch brittle fracture. Welding Res 1953;7:34v–56v.
[9] Shockey DA, Kalthoff JF, Klemm W, Winkler S. Simultaneous measurements of stress intensity and toughness for fast-running cracks in steel. Exp Mech 1983;23:140–5.
[10] Rittel D. Experimental investigation of transient thermoelastic effects in dynamic fracture. Int J Solids Struct 1998;35:2959–73.
[11] Guduru PR, Singh RP, Ravichandran G, Rosakis AJ. Dynamic crack initiation in ductile steels. J Mech Phys Solids 1998;46:1997–2016.
[12] Hutchinson JW. Singular behaviour at the end of a tensile crack in a hardening material. J Mech Phys Solids 1968;16:13–31.
[13] Rice JR, Rosengren GF. Plane strain deformation near a crack tip in a power-law hardening material. J Mech Phys Solids 1968;16:1–13.
[14] Zhou M, Ravichandran G, Rosakis AJ. Dynamically propagating shear bands in impact-loaded prenotched plates – II. Numerical simulations. J Mech Phys Solids 1996;44:1007–32.
[15] Venkert A, Guduru PR, Ravichandran G. An investigation of dynamic failure in 2.3Ni–1.3Cr–0.17C steel. Metall Mater Trans A 2000;31:1147–54.
[16] Zhuang S, Ravichandran G. SM Report No. 98-4, Graduate Aeronautical Laboratories, California Institute of Technology, Pasadena, CA; 1998.
[17] Moss G, Pond Sr RB. Inhomogeneous thermal changes in copper during plastic elongation. Metall Trans A 1975;6A:1223–35.
[18] Costin LS, Crisman EE, Hawley RH, Duffy J. On the localization of plastic flow in mild steel tubes under torsional loading. In: Harding J, editor, Proceedings of the Second Conference on the Mechanical Properties of Materials at High Rates of Strain. London: The Institute of Physics; 1979. p. 90–100.
[19] Hartley KA, Duffy J, Hawley RH. Measurement of the temperature profile during shear band formation in steels deforming at high strain rates. J Mech Phys Solids 1987;35:283–301.
[20] Marchand A, Duffy J. An experimental study of the formation process of adiabatic shear bands in a structural steel. J Mech Phys Solids 1988;36:251–83.
[21] Zehnder AT, Rosakis AJ. On the temperature distribution at the vicinity of dynamically propagating cracks in 4340 steel. J Mech Phys Solids 1991;39:385–415.
[22] Zehnder AT, Rosakis AJ. A note on the use of high speed infrared detectors for the measurement of temperature fields at the vicinity of dynamically growing cracks in 4340 steel. J Appl Mech 1992;59:450–2.
[23] Mason JJ, Rosakis AJ. On the dependence of the dynamic crack-tip temperature fields in metals upon crack-tip velocity and material parameters. Mech Mater 1993;16:337–50.
[24] Zehnder AT, Ramamurthy AC, Bless SJ, Brar NS. Stone impact damage to automotive paint finishes – Measurement of temperature rise due to impact. Int J Impact Engng 1993;13:133–43.
[25] Kallivayalil JA, Zehnder AT. Measurement of the temperature field induced by dynamic crack growth in beta-C titanium. Int J Fracture 1994;66:99–120.
[26] Zhou M, Ravichandran G, Rosakis AJ. Dynamically propagating shear bands in impact-loaded prenotched plates – I. Experimental investigations of temperature signatures and propagation speed. J Mech Phys Solids 1996;44:981–1006.
[27] Hodowany J, Ravichandran G, Rosakis AJ, Rosakis P. Partition of plastic work into heat and stored energy in metals. Exp Mech 2000;40:113–23.

[28] Li Z, Lambros J. Dynamic thermomechanical behavior of fiber reinforced composites. Composites, Part A. Appl Sci Manuf 2000;31:537–47.
[29] Zehnder AT, Guduru PR, Rosakis AJ, Ravichandran G. Million frames per second infrared imaging system. Rev Sci Instrum 2000;71:3762–8.
[30] Narasimhan R, Rosakis AJ. Three-dimensional effects near a crack tip in a ductile three-point bend specimen. Part I. A numerical investigation. J Appl Mech 1990;57:607–17.
[31] Nakamura T, Parks DM. Three-dimensional crack front fields in a thin ductile plate. J Mech Phys Solids 1990;38:787–812.
[32] Rosakis P, Rosakis AJ, Ravichandran G, Hodowany J. A thermodynamic internal variable model for the partition of plastic work into heat and stored energy in metals. J Mech Phys Solids 2000;48:581–607.
[33] Narasimhan R, Basu S. Numerical simulations of fracture initiation in ductile solids under mode I, dynamic loading. Bull Mater Sci 1999;22:891–900.
[34] Rosakis AJ, Freund LB. Optical measurement of the plastic strain concentration at a crack tip in a ductile steel plate. J Engng Mater Technol 1982;104:115–25.
[35] Chiang FP, Hareesh TV. Three-dimensional crack tip deformation: an experimental study and comparison to HRR field. Int J Fracture 1988;36:243–57.
[36] Zehnder AT, Rosakis AJ. 3-Dimensional effects near a crack tip in a ductile 3-point bend specimen. 2. An experimental investigation using interferometry and caustics. J Appl Mech 1990;57:618–26.
[37] Seidler S, Grellmann W. Fracture behavior and morphology of PC/ABS blends. J Mater Sci 1993;28:4078–84.
[38] Couque H. Effect of loading rate on the plane stress fracture toughness properties of an aluminum alloy. Journal de Physique IV 1994;C8-4:747–52.
[39] Winkler SR. Magnetic emission detection of crack initiation. In: Gudas JP, Joyce JA, Hackett EM, editors. Fracture Mechanics: Twenty-First Symposium, ASTM STP 1074, American Society for Testing and Materials, Philadelphia, PA; 1990. p. 178–92.
[40] Joyce JA, Hackett EM. Dynamic *J–R* curve testing of a high strength steel using the key curve and multispecimen techniques. In: Underwood JH, Chait R, Smith CW, Wilhelm DP, Andrews WA, Newman JC, editors. Fracture Mechanics: Seventeenth Volume, ASTM STP 905. American Society for Testing and Materials, Philadelphia, PA; 1986. p. 741–74.